Supplemental Material

Multidimensional Hydrogen Tunneling in Supported Molecular Switches: The Role of Surface Interactions

Yair Litman*

Fritz Haber Institute of the Max Planck Society, Faradayweg 4–6, 14195 Berlin, Germany, and Institute for Chemistry and Biochemistry, Freie Universität Berlin, Arnimallee 22, 14195 Berlin, Germany

Mariana Rossi†

Fritz Haber Institute of the Max Planck Society, Faradayweg 4–6, 14195 Berlin, Germany, and MPI for the Structure and Dynamics of Matter, Luruper Chaussee 149, 22761 Hamburg, Germany

(Dated: October 9, 2020)

* litman@fhi-berlin.mpg.de

† mariana.rossi@mpsd.mpg.de

I. ELECTRONIC STRUCTURE CALCULATIONS

Density functional calculations were performed using the FHI-aims program [1]. The metal surface models were created using the atomic simulation environment ASE [2] and were represented by a slab with a 4×6 surface unit cell including 4 layers and a 70 Å vacuum in the direction perpendicular to the surface. We have only held the bottom two layers fixed and explicitly considered all other degrees of freedom. FHI-aims *light* basis sets and numerical settings were used in the production calculations. Calculations with standard *intermediate* settings were also performed for the Cu and Ag surfaces resulting in deviations smaller than 10 meV. Convergence results with respect to number of layers and k-point sampling of the reciprocal space for all surfaces that were studied are presented in Tab. S1-S7. The settings used in the main text are highlighted in the tables and are in good agreement with previously reported values in Ref. [3] using different exchange correlation functionals (optB86b-vdW, BEEF and vdW-DF-cx).

layers \ k-grid	3x3x1	6x6x1
4	**183**	188
6	194	-
8	188	-
4 (PBE + MBD-nl)	175	-
4 (HSE06 [4]+ vdW [5]	144	-

TABLE S1. Convergence of reaction energy, E(*trans*)-E(*cis*), for the Cu(110) surface. Values are expressed in meV. Unless otherwise specified, the PBE [6] exchange correlation functional augmented with vdW dispersion corrections [5] (vdW^{surf}) was used. MBD-nl refers to the non-local version of the many-body-dispersion method [7], and the exchange correlation functional HSE06 was used with $\omega = 0.11\text{bohr}^{-1}$ [4]. Lattice constant: 3.632Å.

layers \ k-grid	1x1x1	3x3x1	6x6x1
4	**24**	24	-
6	-	31	-
8	-	34	-
4 (PBE + MBD-nl)	-	24	-

TABLE S2. Same as in Tab. S1 but for the Ag(110) surface. Lattice constant: 4.152Å.

layers \ k-grid	3x3x1	6x6x1
4	**356 / 660**	185 / 313
8	346 / 646	-
4 (HSE06 +vdW^{surf})	380 /704	-

TABLE S3. Energy barriers for stepwise / concerted mechanism (respectively) at the Cu(110) surface with different simulation settings. Energies expressed in meV. Values reported for HSE06+vdW^{surf} were calculated at PBE+vdW^{surf} geometries.

layers \ k-grid	1x1x1	2x2x1	6x6x1
4	**188 / 337**	185 / 313	-
8	196 / 342	-	-
4 (HSE06 +vdW^{surf})	250 / 455	-	-

TABLE S4. Same as in Table S3, but for the Ag(110) surface.

layers \ k-grid	3x3x1	6x6x1
4	**75**	72
6	80	-

TABLE S5. Convergence of reaction energy, E(*trans*)-E(*cis*) for Au(110) surface. Lattice constant: 4.157Å. See caption in Tab. S1.

layers \ k-grid	3x3x1	6x6x1
4	**151**	147
6	144	-

TABLE S6. Convergence of reaction energy, E(*trans*)-E(*cis*) for Pd(110) surface. Lattice constant: 3.951Å. See caption in Tab. S1.

layers \ k-grid	3x3x1	6x6x1
4	**209**	210
6	220	-

TABLE S7. Convergence of reaction energy, E(*trans*)-E(*cis*) for Ni(110) surface. Lattice constant: 3.501 Å. See caption in Tab. S1.

II. REACTION AND BARRIER ENERGIES

In Tab. S8, the *cis*→ *trans* energy difference ($\Delta\tilde{E}$), the energy barrier of the stepwise mechanism ($\tilde{E}^*_{\text{step}}$) and the energy barrier of the concerted mechanism ($\tilde{E}^*_{\text{con}}$) for different metallic surfaces are presented. Note that, differently to the values reported in Tab. II in the main text, ΔE and E^*_{step}, the reported values in S8 are not zero-point energy corrected.

Surface	$\Delta\tilde{E}$	$\tilde{E}^*_{\mathrm{step}}$	$\tilde{E}^*_{\mathrm{con}}$
Ag(110)	24	188	313
Au(110)	75	216	386
Cu(110)	183	356	660
Ni(110)	209	498	914
Pd(110)	151	480	822

TABLE S8. Calculated reaction and barrier energies for the DHT of porphycene at several fcc [110] surfaces. Values are not zero-point energy corrected. See definitions in text. Energies are expressed meV.

III. RING POLYMER INSTANTON CALCULATIONS

The ring polymer instanton (RPI) simulations were performed using the implementation created by us in the i-PI package [8, 9]. Several enhancements in the implementation used for these calculations are available in the open-source code repository and described in Ref. [10]. The force convergence criterion for the transition state geometry and instanton optimizations was 0.005 eV/Å. The calculations need to be converged with respect to the number of discretization points of the closed closed Feynman path (CFP), also known as beads. The high-dimensional neural network reported in Ref. [11] which delivers an accurate description of the gas phase porphycene potential energy surface was used to perform such convergence tests due to its reduced computational cost. Since it presents a similar vibrational spectrum to the systems considered here, it shows a comparable convergence behaviour. In Tab. S9 and Tab. S10 the convergence of the hydrogen transfer rates for concerted and stepwise mechanisms, respectively, is presented. The reported rates for the DHT of porphycene on Cu(110) and Ag(110) in Fig. 2 in the main text were calculated with a different number of beads at each temperature, in such way to ensure that the error was always below 20% for the stepwise mechanism and within the order of magnitude for the concerted one.

T(K) \ Beads	128	256	512	1024
90	**0.91**	0.98	1.00	-
60	0.77	**0.95**	1.00	-
30	0.17	0.62	**0.91**	1.00

TABLE S9. Convergence of the reaction rate for the stepwise reaction. For each temperature a value of one is assigned to the converged rate. The number of beads used at each temperature for the instanton rate calculations in this work is highlighted.

T(K) \ Beads	128	256	512	1024	2048
60	**0.82**	0.96	1.00	-	-
30	0.53	**0.79**	0.92	1.00	-
10	-	-	**0.38**	0.69	1.00

TABLE S10. Convergence of the reaction rate for the concerted reaction. For each temperature a value of one is assigned to the calculation with a bigger amount of beads. The number of beads used at each temperature for the instanton rate calculations in this work is highlighted.

IV. CALCULATION OF SURFACE FLUCTUATIONS ENHANCEMENT FACTORS

In absence of rotational degrees of freedom, the RPI reaction rate can be expressed as [12]

$$k_{\text{inst}}(\beta)Q_r(\beta) = \frac{1}{\beta_P\hbar}\sqrt{\frac{\sum_{i=1}^{f}\sum_{k=1}^{P} m_i(\bar{x}_i^{k+1}-\bar{x}_i^{k})^2}{2\pi\beta_P\hbar^2}}\left(\frac{P\sum_{i=1}^{f/3} m_i}{2\pi\beta_P\hbar^2}\right)^{3/2}\prod^{Pf}\frac{1}{\beta_P\hbar|\eta_k|}e^{-S(\bar{\mathbf{x}})/\hbar}, \tag{1}$$

where P is the number of beads, $\bar{x}_i^k$ represents the i-th degree-of-freedom (DOF) of the k-th bead evaluated at the instanton geometry ($\bar{\mathbf{x}}$), f is the number of physical DOF for each bead, m_i is the mass associated to the i-th DOF, S is the Euclidean action, $Q_r(\beta)$ is

the reactant partition function, and $\beta_P = 1/(k_B T P)$ with $k_{\rm B}$ the Boltzmann constant and T the temperature. η_k are the $P \times f$ eigenvalues of the instanton dynamical matrix, and the prime symbol refers to the fact that the modes associated with translational invariance of the "super-molecule" and the mode describing the cyclic permutation of the beads are excluded from the product.

In the "standard" instanton calculations the DOF associated with the atoms of the molecule ($f_{\rm mol}$) and the top two layers of the surface ($f_{\rm surf}$) are allowed to relax during the optimization, and Eq. 1 is evaluated with $f = f_{\rm mol} + f_{\rm surf}$. Thus, the surface fluctuations are automatically included by construction. In order to asses the dynamical surface effects on the double intramolecular hydrogen transfer (DHT), a second set of "constrained" calculations was carried out in which the surface atoms are fixed at the reactant position and only the molecular DOF are optimized. The later set of calculations does not include the fluctuations of the surface DOF resulting on a different instanton geometry, a different Euclidean action, and a different description of the harmonic fluctuations around the instanton pathway, i.e. the prefactor to the exponential in Eq. 1 includes only $f_{\rm mol}$ DOF. The ratio between the "standard" and the "constrained" rates is defined as the "surface fluctuations enhancement" (SFE).

V. MULTIDIMENSIONAL TUNNELING PATHWAYS

In Fig. S1, 3D and 2D projections of the minimum energy pathway (MEP) and the instanton tunneling paths at several temperatures on Cu(110) are presented. The MEP involves a shortening of 0.22 Å of the distance between nitrogen atoms ($d_{\rm NN}$) and a flattening of the molecular conformation, as quantified in Tab. S11. The tunneling paths can be compared with the position of the transition state in the MEP, marked by a triangle. The projections show that decreasing the temperature causes the tunneling path to depart further from the position of the transition state. For example, at 40 K $d_{\rm NN}$ decreases only 0.1 Å in the tunneling path and it passes through a region 75 meV higher in energy than the transition state point. The shortening of the tunnelling pathway is the well-known concept coined as corner cutting. We note that static surface effects that cause the buckling of the *cis* and *trans* conformers on Cu(110) result a considerable increase of the tunneling path length and consequent decrease of $k_{\rm inst}$ with respect to the gas-phase. Similar effects can be observed

in Fig. S2 for the Ag(110) surface.

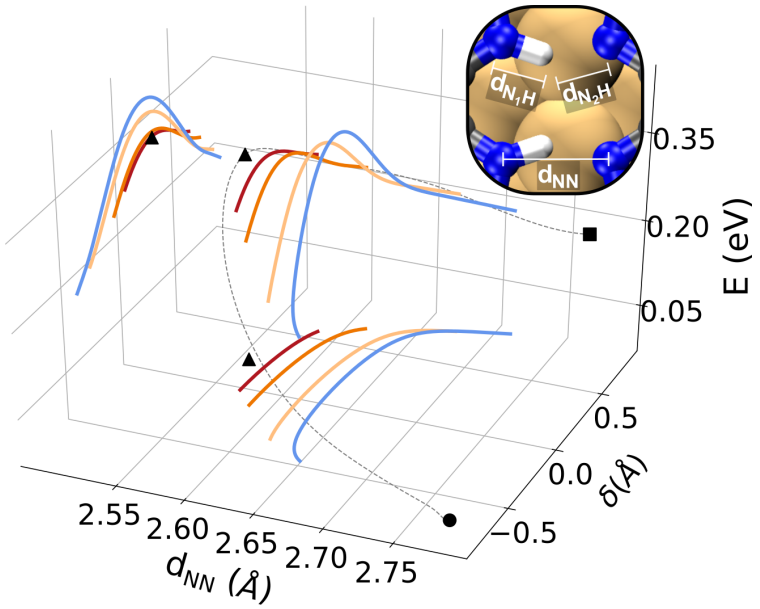

FIG. S1. 3D visualization of the stepwise instanton pathway at Cu(110) at 40 K (blue), 75 K (orange), 150 K (dark orange) and 200 K (red). The *cis*, *trans* and transition state geometries are marked with a circle, square and triangle, respectively. Projections are shown with respect to the nitrogen-nitrogen distance d_{NN}, and the DHT coordinate $\delta = d_{\mathrm{N_1H}} - d_{\mathrm{N_2H}}$. The definition guarantees a value of zero when the hydrogen atom is equidistant from $\mathrm{N_1}$ and $\mathrm{N_2}$. The MEP (grey dashed curve) is also plotted as a reference.

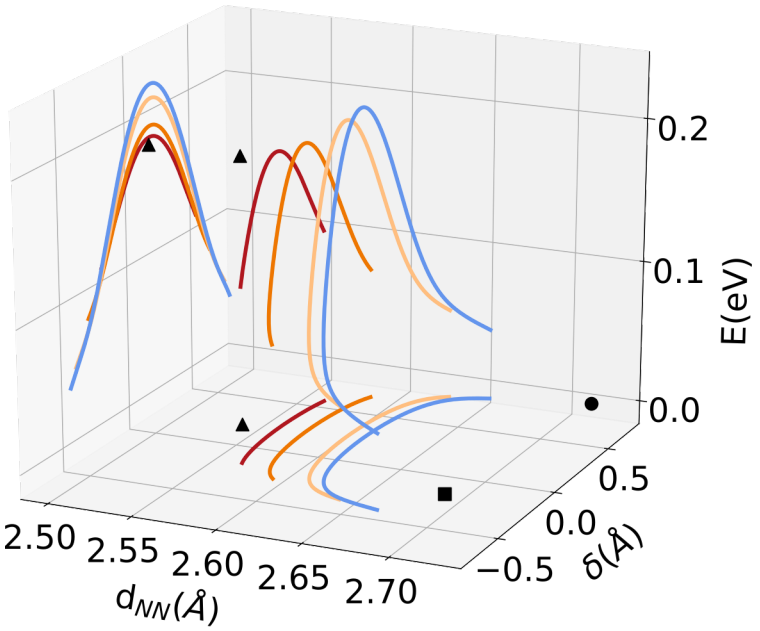

FIG. S2. 3D visualization of the instanton pathway at Ag(110) at 50K (blue), 80K (orange), 150K (dark orange) and 200K (red). The *cis*, *trans* and transition state geometries are represented by black circle, square and triangle, respectively. See coordinates definitions in the caption of Fig. S1.

VI. DETAILS ON THE CALCULATION OF THE DHT ON AG(110)

As discussed in the main text, on Ag(110) at 8.5K the concerted mechanism becomes dominant over the stepwise one. The Euclidean action can be written as $S = \beta\hbar U^{\mathrm{RP}}$, where U^{RP} is the potential energy of the ring polymer which represents the discretization of the closed Feynman path [13]. The exponential dependence that the rate has on $S[\mathbf{x}_{\mathrm{inst}}(\beta)]$ results that at low temperatures (high β values) a small error in S has a huge impact on the rate. For example, an error of only 15 meV produces an error in the rate of $\approx e^{17}$ at 10 K, while at 100 K the error is reduced to only a factor of 5. Thus, while the results for Cu(110) are semi-quantitative, the ones corresponding to the Ag(110) surface at low temperatures should be interpreted only qualitatively.

The *cis* $\rightarrow$ *cis* reaction in the gas phase and on surfaces only admit stationary trajectories that represent second order saddle points rather than first order ones. In a similar spirit to what has been reported in Ref. [14], the steepest descent approximation along the second negative mode can be replaced by the full integration in that direction. This procedure was tested on representative 2D systems performing the required numerical integration using 200

points. The results of this procedure were contrasted with taking the module of the second negative frequency and using the standard expression for the rate. While the results differ by one or two orders of magnitude, the temperature dependence is similar (same order of magnitude). Nevertheless, this effect is minor in comparison to the inaccuracy of several orders of magnitude at low temperatures described before.

VII. HEAVY ATOMS CONTRIBUTION TO THE TUNNELLING PROCESS

In Tab. S11, the tunneling path lengths, computed as the arc length along the instanton pathways, for the different atomic species at several temperatures are presented. As expected, the lower the temperature the higher is contribution from heavy atoms to the tunneling dynamics. Even though the DHT is much slower at Cu(110) than at Ag(110), the tunnelling path lengths are very similar, showing that the molecule-surface interaction strength do not qualitatively modify the reaction pathway.

Species / T(K)	H	C	N	Cu
100	0.54/0.58	0.07/0.06	0.06/0.06	0.01/0.00
75	0.62/0.64	0.09/0.09	0.09/0.09	0.01/0.01
50	0.73/0.72	0.15/0.15	0.16/0.15	0.03/0.02

TABLE S11. Tunnelling path lengths for H, C, N and Cu atomic species for the *cis* $\rightarrow$ *trans* reaction at Cu(110) / Ag(110), respectively. Distances are expressed in Å.

VIII. KINETIC ISOTOPE EFFECTS ON THE CU(110) SURFACE

The fact that the kinetic isotope effect (KIE) predicted by transition state theory (TST) is greater than the one predicted by RPI deserves a closer look. The Eyring TST [15] is given by

$$k_{\mathrm{TST}}(\beta) = \frac{1}{2\pi\beta\hbar}\frac{Q^{\ddagger}}{Q_{\mathrm{r}}}e^{-\beta E^{*}} = A_{\mathrm{TST}}e^{-\beta E^{*}}, \tag{2}$$

where $Q^{\ddagger}$ and Q_{r} refer to the transition state and reactant partition functions, respectively,

E^* to the potential energy barrier, and $\beta = 1/k_B T$ with k_B the Boltzmann constant and T the temperature. RPI can be expressed in a similar way, see for example Eq. 1 in the main text and Eq. 8 in Ref. [12], where the terms entering the prefactor are explicitly given. In the main text the activation energy E_A and prefactor refer to the effective Arrhenius slope, $E_A = -\frac{\partial ln(k)}{\partial \beta}$, and effective Arrhenius prefactor, $A = k/e^{-\beta E_A}$. In Table S12, and in order to allow a rigorous comparison between the considered rate theories, the terms "exponential factor" and "prefactor" refer, instead, to the factors that appear in Eq. 2 above and in Eq. 1 of the main text.

As discussed already in the main text, the behaviour of the DHT rate in the low temperature limit for the stepwise mechanism presents an effective Arrhenius slope with a value of approximately ΔE. In the case of the hydrogen isotopologue, ΔE happens to coincide with E^*_{step} while for the deuterium isotopologue E^*_{step} is 90 meV larger. As a consequence of these energetic relations, and a fortuitous compensation (see Tab. S12), DHT rates predicted by TST for the hydrogen isotopologue are unexpectedly similar to the ones predicted by RPI. However, the rates for the deuterium isotopologue are largely underestimated below the cross-over temperature which results in the observed overestimation of KIE.

T (K)	A_{inst}(Hz)	$e^{-S_{\text{inst}}/\hbar}$	A_{TST} (Hz)	$e^{-\beta \tilde{E}^*_{\text{step}}}$
75	6×10^{17}	1×10^{-20}	3×10^{21}	1×10^{-24}
85	1×10^{17}	2×10^{-18}	4×10^{20}	8×10^{-22}
100	7×10^{16}	3×10^{-16}	2×10^{19}	1×10^{-18}

TABLE S12. Dimensionless exponential factor ($e^{-S_{\text{inst}}/\hbar}$ and $e^{-\beta \tilde{E}^*_{\text{step}}}$) and prefactors ($A_{\text{inst}}$ and A_{TST}) obtained from RPI and TST simulations, respectively. $\tilde{E}^*_{\text{step}}$ represents the energy barrier for the stepwise mechanism without zero-point energy corrections, because the exponential factor including these corrections is formally in A_{TST}. Interestingly, even though both theories predict similar DHT rates in this temperature range, the corresponding factors differ significantly.

IX. ESTIMATION OF TRANSITION TEMPERATURE FROM STEPWISE TO CONCERTED MECHANISM IN THE DEEP TUNNELING REGIME

The low temperature behaviour of the DHT rate for the stepwise mechanism can be expressed by an Arrhenius-like formula

$$k_{\mathrm{step}}^{T\to 0}(\beta) \approx A_{\mathrm{step}} e^{-\beta E_A}, \tag{3}$$

where the zero-point energy corrected reaction energy, (ΔE in Tab. II.), is a good approximation of the effective activation energy, E_A, and the prefactor, A_{step}, can be approximated by the values obtained from the instanton calculations performed on the Ag(110) and Cu(110) surfaces. On the contrary, the plateau at the low temperature limit of the rate for the concerted mechanism is difficult to obtain (see Sec. VI). Since this reaction is symmetric, a rough estimate of the rate can be obtained from its tunneling splitting, Δ, as

$$k_{\mathrm{con}}^{T\to 0} \approx \frac{\Delta}{2\pi}. \tag{4}$$

A reasonable 1D approximation of the potential energy along the reactive coordinate can be written as,

$$V(x) = V_0 \left[1 - \left(\frac{x}{x_0} \right)^2 \right]^2, \tag{5}$$

where V_0 is taken as the reaction energy barrier ($\tilde{E}^*_{\mathrm{con}}$ in Tab. S8), and x_0 is a measure of the barrier width that has to be determined.

In Tab. S13, the molecular distortions h_{bu}, measured as the difference between the height of the amino and imino N atoms in the molecule, are presented for the *cis*, the *trans* and transition state geometry corresponding to the concerted reaction at several surfaces. At all surfaces considered, the molecule has to reach a flat conformation, characterized by $h_{\mathrm{bu}} = 0$, for the reaction to take place. $x_0^{\mathrm{Ag}} = 1.2$ Å and $x_0^{\mathrm{Ag}} = 3.0$ Å reproduce Δ values which, by the application of Eq. 3, deliver the experimental and the theoretical plateau rates, respectively. The parameters for other surfaces were obtained by scaling x_0^{Ag} with the ratio of the h_{bu} values reported in Tab. S13, i.e. $x_0^{\mathrm{X}} = x_0^{\mathrm{Ag}} \times (h_{\mathrm{bu}}^{\mathrm{X}}/h_{\mathrm{bu}}^{\mathrm{Ag}})$. Other scaling factors

System	$h_{\rm im}^{cis}$	$h_{\rm am}^{cis}$	$h_{\rm bu}^{cis}$	$h_{\rm im}^{trans}$	$h_{\rm am}^{trans}$	$h_{\rm bu}^{trans}$	$h_{\rm im}^{TS}$	$h_{\rm am}^{TS}$	$h_{\rm bu}^{TS}$
Ag(110)	2.11	2.55	0.44	2.26	2.42	0.16	2.32	2.32	0.0
Au(110)	2.02	2.54	0.52	2.26	2.42	0.16	2.34	2.34	0.0
Cu(110)	1.79	2.38	0.59	1.91	2.23	0.32	2.13	2.13	0.0
Pd(110)	1.68	2.25	0.56	1.78	2.10	0.32	2.06	2.06	0.0
Ni(110)	1.60	2.20	0.60	1.71	2.10	0.39	1.86	1.86	0.0

TABLE S13. Average height of nitrogen atoms belonging to the amino groups ($h_{\rm am}$) and imino groups ($h_{\rm im}$). The geometrical descriptors on columns 2-4, 5-7 and 8-11 correspond to the *cis*, the *trans* and the concerted transition state geometry (TS), respectively. $h_{\rm bu} = h_{\rm am} - h_{\rm im}$ is a measure of the molecular distortion (buckling) [16]. Distances are expressed in Å.

based on the mass-scaled displacement between the *cis* adsorption conformation and a flat conformation were also tested with similar results.

Finally, the tunnelling splittings were computed using the Wentzel-Kramers-Brillouin (WKB) approximation [17], and the transition temperature T_t is derived by setting $k_{\rm con}^{T\to 0} = k_{\rm step}^{T\to 0}$. Both values of T_t, calculated from the experimentally derived parameters and from the theoretically derived parameters, are reported in Tab. II in the main text, giving the reader an assessment of the uncertainty of the estimation. The lower (higher) temperatures correspond to the calculation where the theoretical (experimental) Ag(110) rate value was used as a reference.

X. IMPACT OF VDW INTERACTIONS ON ADSORPTION

In Tab. S14, the reaction energies and geometrical descriptors obtained with the PBE exchange correlation functional without inclusion of vdW dispersion corrections are shown. In passing, we note that in all the systems considered here the pyrrole rings with amino groups are parallel to the surface at a distance equal to $h_{\rm am}$. By comparison with the results reported in Tab. S8 and in Tab. S13, it can be observed that the inclusion of vdW interactions causes the reaction energies to change in most of the cases by 20 % or less, the adsorption geometries are 0.05-0.15 Å closer to the surface, and the geometries are slightly less buckled.

These geometrical changes are more pronounced for the coinage metals (Cu, Ag and Au), indicating that in those surfaces the vdW interactions are somewhat more important. As already found in other hydrogen bonded systems [18], even if small geometrical changes are observed in local minima structures, appreciable differences on the energy barriers can take place. In particular, the decrease of the molecular buckling suggests a decrease of the hydrogen transfer energy barrier, and the decrease of the adsorption heights points towards an increase of the enhancement of the reaction rate due to surface fluctuations.

System	$\Delta\tilde{E}$	h_{im}^{cis}	h_{am}^{cis}	h_{bu}^{cis}	h_{im}^{trans}	h_{am}^{trans}	h_{bu}^{trans}
Ag(110)	0.034	2.18	2.68	0.50	2.36	2.53	0.17
Au(110)	0.060	2.11	2.57	0.57	2.41	2.55	0.13
Cu(110)	0.184	1.87	2.52	0.64	2.06	2.36	0.30
Pd(110)	0.162	1.71	2.30	0.59	1.82	2.14	0.33
Ni(110)	0.183	1.68	2.28	0.60	1.76	2.16	0.40

TABLE S14. Calculated reaction energies, molecular distortions and molecular heights obtained with the PBE exchange correlation functional (without inclusion of vdW dispersion corrections) for the DHT of porphycene. The geometrical descriptors on columns 3-5 and 6-8 correspond to the *cis* and *trans* tautomer respectively. See definitions in Tab. S8 and in Tab. S13. Energies and distances are expressed in meV and Å, respectively.

[1] V. Blum, R. Gehrke, F. Hanke, P. Havu, V. Havu, X. Ren, K. Reuter, and M. Scheffler, Comp. Phys. Comm. **180**, 2175 (2009).

[2] A. H. Larsen, J. J. Mortensen, J. Blomqvist, I. E. Castelli, R. Christensen, M. Dułak, J. Friis, M. N. Groves, B. Hammer, C. Hargus, E. D. Hermes, P. C. Jennings, P. B. Jensen, J. Kermode, J. R. Kitchin, E. L. Kolsbjerg, J. Kubal, K. Kaasbjerg, S. Lysgaard, J. B. Maronsson, T. Maxson, T. Olsen, L. Pastewka, A. Peterson, C. Rostgaard, J. Schiøtz, O. Schütt, M. Strange, K. S. Thygesen, T. Vegge, L. Vilhelmsen, M. Walter, Z. Zeng, and K. W. Jacobsen, J. Phys. Condens. Matter **29**, 273002 (2017).

[3] M. Koch, M. Pagan, M. Persson, S. Gawinkowski, J. Waluk, and T. Kumagai, J. Am. Chem. Soc. **139**, 12681 (2017).

[4] A. V. Krukau, O. A. Vydrov, A. F. Izmaylov, and G. E. Scuseria, J. Chem. Phys. **125**, 224106 (2006).

[5] V. G. Ruiz, W. Liu, E. Zojer, M. Scheffler, and A. Tkatchenko, Phys. Rev. Lett. **108**, 146103 (2012).

[6] J. P. Perdew, K. Burke, and M. Ernzerhof, Phys. Rev. Lett. **77**, 3865 (1996).

[7] J. Hermann and A. Tkatchenko, Phys. Rev. Lett. **124**, 146401 (2020).

[8] M. Ceriotti, J. More, and D. E. Manolopoulos, Comp. Phys. Comm. **185**, 1019 (2014).

[9] V. Kapil, M. Rossi, O. Marsalek, R. Petraglia, Y. Litman, T. Spura, B. Cheng, A. Cuzzocrea, R. H. Meißner, D. M. Wilkins, B. A. Helfrecht, P. Juda, S. P. Bienvenue, W. Fang, J. Kessler, I. Poltavsky, S. Vandenbrande, J. Wieme, C. Corminboeuf, T. D. Kühne, D. E. Manolopoulos, T. E. Markland, J. O. Richardson, A. Tkatchenko, G. A. Tribello, V. V. Speybroeck, and M. Ceriotti, Comp. Phys. Comm. **236**, 214 (2019).

[10] Y. Litman, *Tunneling and Zero-Point Energy Effects in Multidimensional Hydrogen Transfer Reactions: From Gas Phase to Adsorption on Metal Surfaces*, Ph.D. thesis, Freie Universität Berlin (2020).

[11] Y. Litman, J. Behler, and M. Rossi, Faraday Discuss. **221**, 526 (2020).

[12] A. N. Beyer, J. O. Richardson, P. J. Knowles, J. Rommel, and S. C. Althorpe, J. Phys. Chem. Lett. **7**, 4374 (2016).

[13] J. O. Richardson, Int. Rev. Phys. Chem. **37**, 171 (2018).

[14] Y. Zhang, J. B. Rommel, M. T. Cvitaš, and S. C. Althorpe, Phys. Chem. Chem. Phys. **16**, 24292 (2014).

[15] H. Eyring, J. Chem. Phys. **3**, 107 (1935).

[16] T. Kumagai, J. N. Ladenthin, Y. Litman, M. Rossi, L. Grill, S. Gawinkowski, J. Waluk, and M. Persson, J. Chem. Phys. **148**, 102330 (2018).

[17] A. Garg, Am. J. Phys. **68**, 430 (2000).

[18] Y. Litman, D. Donadio, M. Ceriotti, and M. Rossi, J. Chem. Phys. **148**, 102320 (2018).